© 2017 IEEE. Personal use of this material is permitted. Permission from IEEE must be obtained for all other uses, in any current or future media, including reprinting/republishing this material for advertising or promotional purposes, creating new collective works, for resale or redistribution to servers or lists, or reuse of any copyrighted component of this work in other works.

Digital Object Identifier (DOI): 10.1109/TIA.2017.2772198

IEEE Transactions on Industry Applications, 2017

Thermal Stress Based Model Predictive Control of Electric Drives

Johannes Falck
Giampaolo Buticchi
Marco Liserre

Suggested Citation

J. Falck, G. Buticchi and M. Liserre, "Thermal Stress Based Model Predictive Control of Electric Drives," *IEEE Transactions on Industry Applications*, vol. 54, no. 2, pp. 1513-1522, Nov. 2017.

Thermal Stress Based Model Predictive Control of Electric Drives

Johannes Falck, *IEEE Student Member*, Giampaolo Buticchi, *IEEE Senior Member*, Marco Liserre, *IEEE Fellow*
Chair of Power Electronics, Faculty of Engineering
Christian-Albrechts-Universität zu Kiel, Kaiserstr. 2, 24143 Kiel, Germany
Email: jofa@tf.uni-kiel.de, gibu@tf.uni-kiel.de, ml@tf.uni-kiel.de

***Abstract*—The reliable operation of the power electronics system of an electric drive is a critical design target. Thermal cycling of the semiconductors in the power module is one of the main stressors. Active thermal control is a possibility to control the junction temperatures of power modules in order to reduce the thermal stress. In this paper, the finite control set model predictive control (FCS-MPC) is designed for thermal stress based driving of electric drives converters. The optimal switching vector is selected using a multi-parameter optimization that includes the current reference error, the additional thermal stress that a specific switching vector applies to each semiconductor, the temperature spread between semiconductors in the module, overall efficiency and device constraints. This enables relieving the stress due to thermal cycles and reducing unsymmetrical fatigue of the modules chips while avoiding unnecessary losses. The approach is derived in theory and applied in simulation and experiment.**

***Index Terms*—Finite Control Set Model Predictive Control, Active Thermal Control, Junction Temperature Estimation, Lifetime Prediction, Power Electronics Reliability**

I. Introduction

Power semiconductors are increasingly used not only in traditional fields like variable speed drives, consumable electronics and in new but consolidated ones like renewable energies but also in emerging fields like more-electric aircrafts and medical systems. Presently, the control system technology finds itself in a paradigm-changing tipping point, in which more demanding control goals, system flexibility, and functionalities required by emerging applications are driving the control system technology development, in addition to stabilization and robustness, which was the main focus in the past [1]. The reliable operation is becoming crucial for the safety of several key areas like energy, health and transportation [2]. To reduce the required system size, material consumption and working time, power semiconductors in the lower and medium power range are often assembled into modules [3], [4]. An important cause of aging and failures of these modules is the cyclic heating and cooling processes, so called thermal cycles [5]. Manufacturers face this problem by improving the assembly and materials which suffer from mechanical fatigue [6]. These solutions attempt at reducing the effects of thermal cycling without curing the cause of the problem.

Only limited research has been carried out to reduce the thermal cycling with active thermal control, which aims at smoothing the fluctuation of the junction temperature of the semiconductors during operation [7]. Chosen control variables are the switching frequency [8], the modulation method [9], the dc link voltage [10], reactive circulating current [11], [12], the active circulating current [13], the turn on rise times [14] and balancing of the thermal stress in a modular structure [15]. However, the main disadvantage of active thermal control is the decrease of the overall system efficiency or system performance [16]. In addition to the performance deterioration, additional thermal control loops increase the complexity and the accumulated damage of the semiconductor is not taken into account.

This paper presents a control approach that aims at overcoming these limitations to widen the use of active thermal control in power electronic applications, especially for electric drives. For this purpose finite control-set model predictive control (FCS-MPC) seems the optimal approach because it allows an optimal control of every switching event and including of non-linear thermal and lifetime related models into the control law. A precise control of the thermal stress in the semiconductors can be achieved as the optimal switching vector is directly applied to the physical system. A model for online junction temperature estimation that is suited for the use of FSC-MPC is designed. The proposed algorithm is a software solution for increasing the reliability and does not utilize special hardware like extra temperature probes nor active gate drivers.

In the following the Model Predictive Control is introduced in section II and the active thermal control is introduced in section III. The algorithm using FCS-MPC to control the junction temperatures is described and validated in simulation and experiment in section IV. A conclusion is given in section V.

II. Model Predictive Control

Predictive control has been proposed in power electronics systems for more than 30 years [17], [18]. Its strength are demanding control goals that require non-linear models or multiple control variables [1].

The main principle of MPC is to use a model of the system to predict its dynamic behaviour during operation. The system outputs are computed by evaluation of a cost function based on this prediction. Fig. 1 shows the general structure of MPC. The main parts are the system model, the cost function and the control law which is derived from the optimizer [19]. The

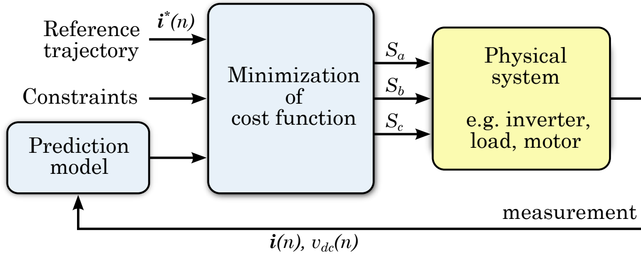

Fig. 1. Control Structure of FCS-MPC using the receding horizon principle.

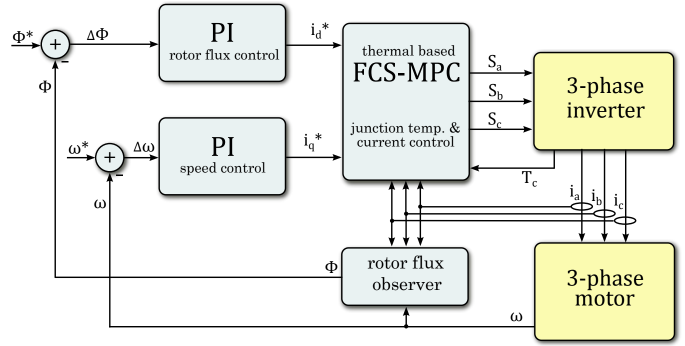

Fig. 2. Control Structure of 3-phase permanent magnetized synchronous machine. T_c is a low-bandwidth measurement of the case temperature which is used as an input to the junction temperature estimation.

system model holds electrical and thermal information of the converter, that are necessary to predict current and temperature progression. The calculation of the system outputs is done using the receding horizon principle. To this, the optimal future output is evaluated each sample and subsequent it is applied to the system. In the next sample, this calculation is repeated using updated measurement inputs. This ensures a feedback, making MPC a type of closed-loop control [20].

Switching elements in power electronic systems can be driven either by using a modulator or the switching signals are generated directly by the controller. As only a finite amount of switching states is possible in power electronic inverters, the latter can be realized using FCS-MPC. This is advantageous as no modulator is needed and every switching operation can be determined by the cost function of the control algorithm. Therefore, the switching frequency is variable.

Assuming a three-phase two-level voltage source inverter (VSI) topology, as it is used in a variety of applications in electric drives or grid injection, a total amount of $2^3 = 8$ space vectors (SV) is possible. From these valid switching states, six are active and two are zero vectors. In FCS-MPC, the model is used to predict the consequences of each possible switching operation to the depth of the prediction horizon. The cost function is used to evaluate which switching operation is optimal and it is then applied to the physical system.

The FCS-MPC can be applied to control the motor current in a cascaded control of an induction motor. Rotor flux and machine speed are controlled in a field oriented control scheme using PI controllers. The full scheme of the 3-phase motor control is given in Fig. 2.

III. Junction Temperature Control

Junction temperature control methods smooth the junction temperature progression in the module's semiconductors during operation. Their goal is to keep the thermal swing as small as possible [21]. Therefore, thermo-mechanical stress is released from the semiconductor chips which leads to increased lifetime of the module [6], [22].

A. Active Thermal Control

Present junction temperature control methods can be classified in two main approaches: The first is to alternate the power losses in the semiconductors while maintaining the application's mission profile. By applying additional losses in the module, the temperature can be raised temporary or vice versa reducing the losses decreases the temperature temporary. Variation of parameters like the switching frequency or the intermediate circuit dc voltage allow alternating the losses and fulfilling the mission profile demand. As the losses are controlled active during operation, this method is called active thermal control [8]. The second approach is to optimize the mission profile for a better thermal behavior of the hardware components [7]. In both cases, the thermal stress is relieved in the module and the aging can be reduced.

B. Junction Temperature estimation

The knowledge of the junction temperatures is necessary to apply active thermal control. However, measurements that meet the bandwidth demand for the control are challenging. Therefore, several temperature sensitive electrical parameters (TSEP) have been introduced to obtain the chip temperatures [23]. A less invasive method is to use model-based estimations of the junction temperatures. The junction temperature estimation is based on power loss calculations and the thermal properties of the device's cooling path. Both can be described in models for online calculation. This has been presented for PWM based control systems in [24].

The FCS-MPC is a direct control without use of a modulator and with a variable switching frequency. Thus, the existing model is not applicable. An adapted junction temperature estimation model shown in Fig. 3 is designed next using a power loss calculation and a thermal network: The conduction losses are calculated using the v_{ce} characteristic of the semiconductors and the collector current i_c, which is derived from a measurement of the phase current. The switching losses are given with the switching energy characteristics E_{on} and E_{off} of the semiconductors and the sampling time. Switching of the device is determined by the FCS-MPC algorithm and therefore, all switching operations are known to the control. The switching energy loss is only considered if a switching occurs and is set to zero otherwise.

A linear Cauer-type thermal network as applied in [24] is used to calculate the temperatures that occur in the module's layers based on the power losses, a low-bandwidth temperature

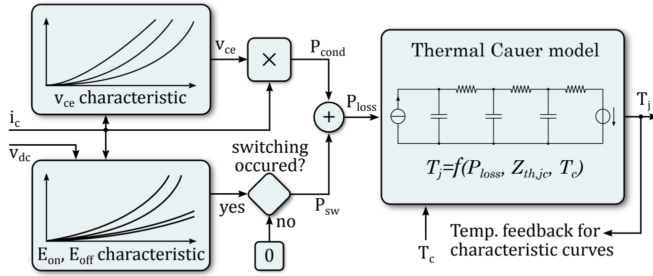

Fig. 3. Online junction temperature estimation model for FCS-MPC.

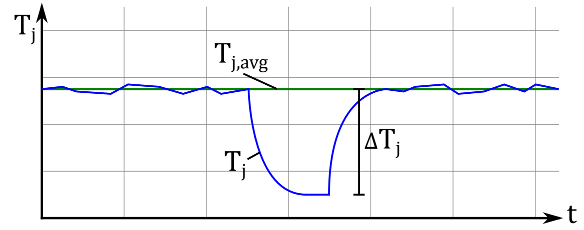

Fig. 4. Thermal cycle amplitude definition using the junction temperature and its long-term average value.

measurement of the modules case T_c that is often included in packages and the thermal impedance between junction and case $Z_{th,jc}$. This enables to estimate the junction temperatures.

To apply active thermal control, a criterion for the thermal cycle amplitude ΔT_j is mandatory. It is based on the junction temperature estimation T_j and its average value $T_{j,avg}$.

$$\Delta T_j = T_j - T_{j,avg} \tag{1}$$

This is displayed in Fig. 4. Positive values of ΔT_j indicate thermal cycles above the average temperature whereas negative values indicate thermal cycles below it. The average is created using a low-pass filter with a time constant adjusted to maximum length of a thermal cycle that has to be reduced by the thermal controller (i.e. $\tau = 60\,\text{s}$).

C. Lifetime Estimation

The main failure mechanisms of power semiconductor modules are induced by plastic strain of inside interconnections caused by temperature cycling. The most vulnerable interconnections are the bond wire fixation and the chip solder [25]. In the 1990s the LESIT study was conducted to quantify the effect of power cycling on the modules using accelerated lifetime tests [25]. In order to relate the failure mechanisms and quantified reliability performance, several models have been proposed. These are based on the Coffin-Manson model that describes the occurrence of plastic deformation due to a periodic process. The Coffin-Manson-Arrhenius model considers temperature cycling and average temperature based on the LESIT results [26]. The Norris-Landzberg Model additionally takes into account the cycling frequency of the junction temperature [27]. The CIPS 2008 model [28] also includes more specific parameters on the operating conditions. Its analytical equation is:

$$N_f = A \cdot \Delta T_j^{\beta_1} \cdot exp\left(\frac{\beta_2}{T_{j,min}}\right) \cdot t_{on}^{\beta_3} \cdot i_B^{\beta_4} \cdot V_C^{\beta_5} \cdot d_b^{\beta_6} \tag{2}$$

The number of cycles to failure N_f is described in dependency of the amplitude of thermal cycles ΔT_j and the average temperature $T_{j,avg}$. Other coefficients consider the pulse duration t_{on}, the current per bond foot i_B, the voltage class V_C, the bond wire diameter d_b and a technology factor A. The coefficients β_{1-6} are extracted from a data set of multiple reliability experiments and is adjusted for best match a three-phase inverter IGBT module ($i_{max} = 25\,\text{A}$, $v_{dc,max} = 1200\,\text{V}$) that is used for the experimental validation using data provided in datasheets and application manuals. The equation is derived using the coefficients in Table I.

TABLE I
PARAMETERS FOR CIPS 2008 MODEL

Parameter	Symbol	Value	Coefficient
Technology Factor	A	$2.03 \cdot 10^{14}$	n.a.
Temperature difference	ΔT	variable	$\beta_1 = -4.416$
Min. chip temperature	$T_{j,min}$	variable	$\beta_2 = 1285$
Pulse duration	t_{on}	variable	$\beta_3 = -0.463$
Current per bond foot	i_B	$i_c/4$ bonds	$\beta_4 = -0.716$
Voltage class /100	V_C	12 V	$\beta_5 = -0.761$
Bond wire diameter	d_b	300 μm	$\beta_6 = -0.5$

To achieve a quantity of the damage taken by a specific thermal cycle the reciprocal of N_f is applied. If almost no junction temperature cycling takes place or noise occurs in the estimation N_f^{-1} is close to zero. For larger thermal cycles the damage rises according to the exponential influence of ΔT_j. The weighting of harmful temperature cycles makes N_f^{-1} a good choice as an input to the active thermal controller.

To consider multiple thermal cycles with multiple properties as they occur in most applications, Miners cumulative damage rule is applied [29]. Miners rule can be written as:

$$c = \sum_i N_{f,i}^{-1} \tag{3}$$

Here c is the cumulative damage, which rises the more thermal cycles occur in operation.

IV. FCS-MPC TO REDUCE THERMAL STRESS

Active thermal control can benefit from the non-linear control structure of MPC. Additional, FCS-MPC offers the possibility to apply a particular space vector directly to the inverter system as no modulator is used in this control structure. In this section, the proposed procedure is developed first. Secondly, the effectiveness is demonstrated using simulation. In the end, experimental results are given to validate the behavior using an infrared camera.

A. Thermal-based MPC procedure

The purpose of the algorithm is to keep the fatigue of the module low by reducing the thermal stress. In contrast to other active thermal control studies, it also allows to equalize

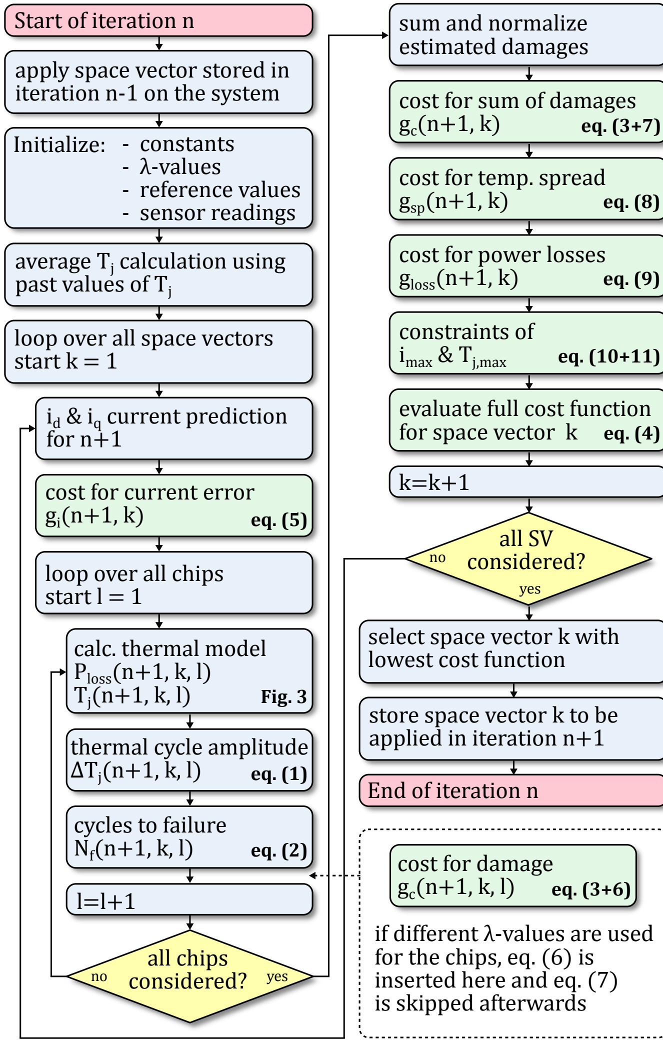

Fig. 5. Flow chart of the proposed thermal-based FCS-MPC procedure.

the junction temperatures in the power module. The power losses are changed according to the stress that results from thermal cycles. The gain is adjusted using λ-coefficients that are introduced in this section. This allows tuning to have the maximum allowed power losses in the case of the maximum thermal stress. When the cycle ends, its amplitude vanishes and operation is reset to normal. This behavior actually limits the increase of the additional power losses that may be introduced by other active thermal control studies.

The FCS-MPC allows predicting the current, power losses, junction temperatures and accumulated damage for all possible space vectors at each sampling instant. The principle of the FCS-MPC is to predict these parameters for sample time instants n and space vectors k and score each prediction using a cost function. To choose the most suitable space vector for the next sampling instant the minimal cost function is searched. As no modulator is used, this space vector is directly applied to the system.

The flow chart of the procedure is given in Fig. 5 for iteration n which corresponds to a one-step prediction horizon.

TABLE II
PREDICTED COST FUNCTION ELEMENTS

Cost function element	Gain	Symbol
Error from current reference	λ_i	$g_i(n,k)$
Additional device damage	$\lambda_{c,l}$	$g_c(n,k,l)$
Device junction temperature spread	λ_{sp}	$g_{sp}(n,k)$
Power losses (switching & conduction)	λ_{loss}	$g_{loss}(n,k)$
Maximum device current constraint	-	$g_{imax}(n,k)$
Maximum device temperature constraint	-	$g_{Tmax}(n,k)$

To increase the prediction horizon, the procedure has to be executed again for each resulting space vector. The execution of the procedure can be time consuming, especially if the prediction horizon is increased. For this reason, in iteration n the calculation of the optimal space vector is done for the next iteration $n+1$ and it is applied on the converter at beginning of that iteration.

The cost function that needs to be minimized consists of a compilation of all quantities that are involved in the optimization:

$$g(n,k) = g_i(n,k) + g_c(n,k) + g_{sp}(n,k) + g_{loss}(n,k) + g_{imax}(n,k) + g_{Tmax}(n,k) \tag{4}$$

The symbols of the cost function equation are given in Table II. For the proposed thermal-based control it includes elements for the current reference error, the amount of damage that a thermal swing adds to the module, the spread of junctions temperatures from a mean value and the amount of energy that is necessary for the predicted switching operation. The elements of the cost function are weighted by λ-coefficients to make it tunable for the desired application. Additional constraints for the maximum device current and the maximum junction temperature are added. The cost function elements are established in the following for each part in particular.

First part is the current reference error. Typically the absolute value of current error to its reference value is chosen for both, d and q component of the current [30]. The cost function element for the current error g_i is denoted as:

$$g_i(n,k) = \lambda_i \cdot (|i_d^* - i_{d,k}| + |i_q^* - i_{q,k}|) \tag{5}$$

In this equation i_d^* and i_q^* are the current reference values and $i_{d,k}$ and $i_{q,k}$ are the predicted currents for the applied space vector k in the dq-frame. The current reference is assumed to be constant for sampling instant n.

Next, the additional damage for each semiconductor l in the module is computed for each space vector k using the CIPS 2008 lifetime model of equation (2). The thermal swing ΔT_j is the main parameter in the model. To detect the current amount of thermal swing, the deviation from the junction temperatures average value $T_{j,avg}^l$ are computed according Fig. 4. The base temperature of the thermal swing $T_{j,min}$ is the minimal temperature of a thermal cycle. For the cost function each term is weighted with $\lambda_{c,l}$.

$$g_c(n,k,l) = \lambda_{c,l} \cdot N_{f,n,k,l}^{-1} \tag{6}$$

The calculation of g_c relies on a calculation of the number of cycles to failure N_f for the predicted space vector using the predictions of current and temperature as well as the constant values given in table I. The reciprocal of N_f is a snapshot of the damage at the given time instant. As the starting and ending of thermal cycles are not detected in this procedure it is only suitable for computational light online damage estimation. It ensures that thermal cycles are scored by their potential damage to the semiconductors. A more precise but computational more demanding procedure is the online rainflow counting [31]. It is also suitable for accumulating damage calculation to estimate the consumed lifetime.

Different values for $\lambda_{c,l}$ can be used to quantify the stress that should be relieved from semiconductor l. This enables to equalize the damage in the semiconductors of the module, by relieving the more used ones. However, if this is not used, the dependency from l can be removed by using the average of all q chips on the module:

$$g_c(n,k) = \lambda_c \cdot \frac{1}{q} \sum_{l=1}^{q} g_c(n,k,l), \quad \forall \lambda_{c,l} = 1 \tag{7}$$

Another element of the cost function allows to reduce or to favor the usage of selected semiconductors of the module. This can be used to relive stress from semiconductors that have been particularly stressed before. It also enables to equalize unequal temperatures in the module. The cost function of space vectors that include the selected semiconductor are evaluated higher or lower according to the control goal:

$$g_{sp}(n,k) = \lambda_{sp} \cdot \mathrm{Var}\left(T_{j,l}(n+1,k)\right) \tag{8}$$

The variance of the predicted junction temperatures of all semiconductors l is used to measure how equal the junction temperatures in the module are after applying space vector k. Thus, the cost function element returns low costs for less spread junction temperatures in the module.

The next part of the cost function includes the efficiency, which means reduction of the occurring losses. The dominating losses in the module are the conduction losses and the switching losses [4]. The switching losses can be reduced by choosing space vectors that are neighbored to the previous vector as less semiconductors have to change conductivity [32].

$$g_{loss}(n,k) = \lambda_{loss} \cdot \sum_{l=1}^{q} \left(P_{sw,l}(n,k) + P_{cond,l}(n,k)\right) \tag{9}$$

The calculation of the switching losses and conduction losses is given in Fig. 3.

The last two elements of the cost function are constraints that ensure the safe operation of the inverter. If the condition of a constraint applies, the space vector must not be applied to the system. The cost function's value is set to infinity. For this reason constraints do not have λ-coefficients. If no space vector can be applied the inverter trips.

$$g_{imax}(n,k) = \begin{cases} 0 & |i(n,k)| \leq i_{max} \\ \infty & \text{else} \end{cases} \tag{10}$$

TABLE III
DEFINITION OF λ-PARAMETERS FOR SIMULATION

Cost function element	Value	Cost	λ-Parameter
Current reference error	2 A	$g_i = 0.5$	$\lambda_i = 0.25$
Additional damage	10^{-7}	$g_c = 0.25$	$\lambda_{c,l} = 2.5 \cdot 10^{-6}$
Temperature variance	3 K	$g_{sp} = 0.15$	$\lambda_{sp} = 0.05$
Power losses	200 W	$g_{loss} = 0.1$	$\lambda_{loss} = 5 \cdot 10^{-6}$

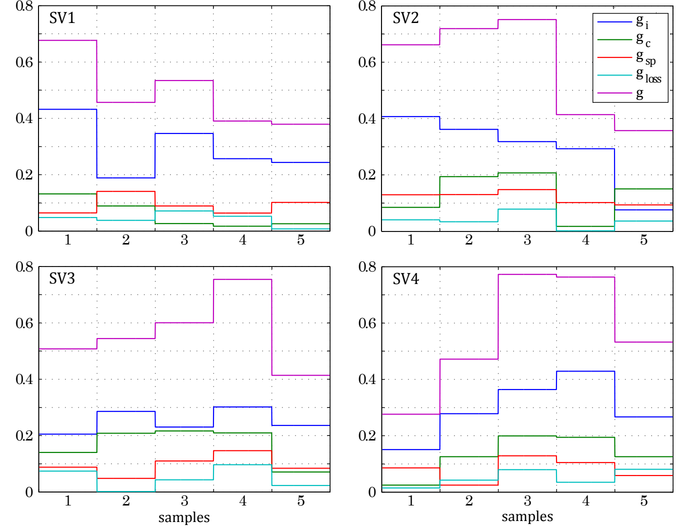

Fig. 6. Set of cost function elements for four space vectors and five samples.

$$g_{Tmax}(n,k) = \begin{cases} 0 & T_j(n,k) \leq T_{j,max} \\ \infty & \text{else} \end{cases} \tag{11}$$

The cost function is evaluated for all space vectors k. The space vector with the minimal cost is then applied to the system. The λ-coefficients allow to tune the behavior of the control. Decreasing of λ_c and λ_{sp} i.e. will reduce the impact of the thermal control. An example for defining the λ-parameters is given in table III. For instance a current error of 2 A is defined to result in a cost of $g_i = 0.5$ and therefore must be set to $\lambda_i = 0.25$. Guidelines for selecting of the λ-coefficients are given in section IV-E in the experimental results.

The optimization of the cost function is illustrated in an example in Fig. 6. To keep it simple, only four of the eight possible space vectors are depicted. If only the cost for current error g_i is minimized, the switching sequence would be 4-1-3-1-2, as space vector 4 has the lowest cost for the current reference error in the first time sample, space vector 1 in the second sample and so on. To find the optimal switching sequence the whole cost function g is minimized. It is the sum of the weighted elements g_i, g_c, g_{sp} and g_{loss}. The resulting switching sequence for the minimal cost function g is 4-1-1-1-2.

B. Evaluation of the FCS-MPC for thermal control

The FCS-MPC with junction temperature control has been applied in simulation for the control of an induction motor. Rotor flux and machine speed are controlled in a field ori-

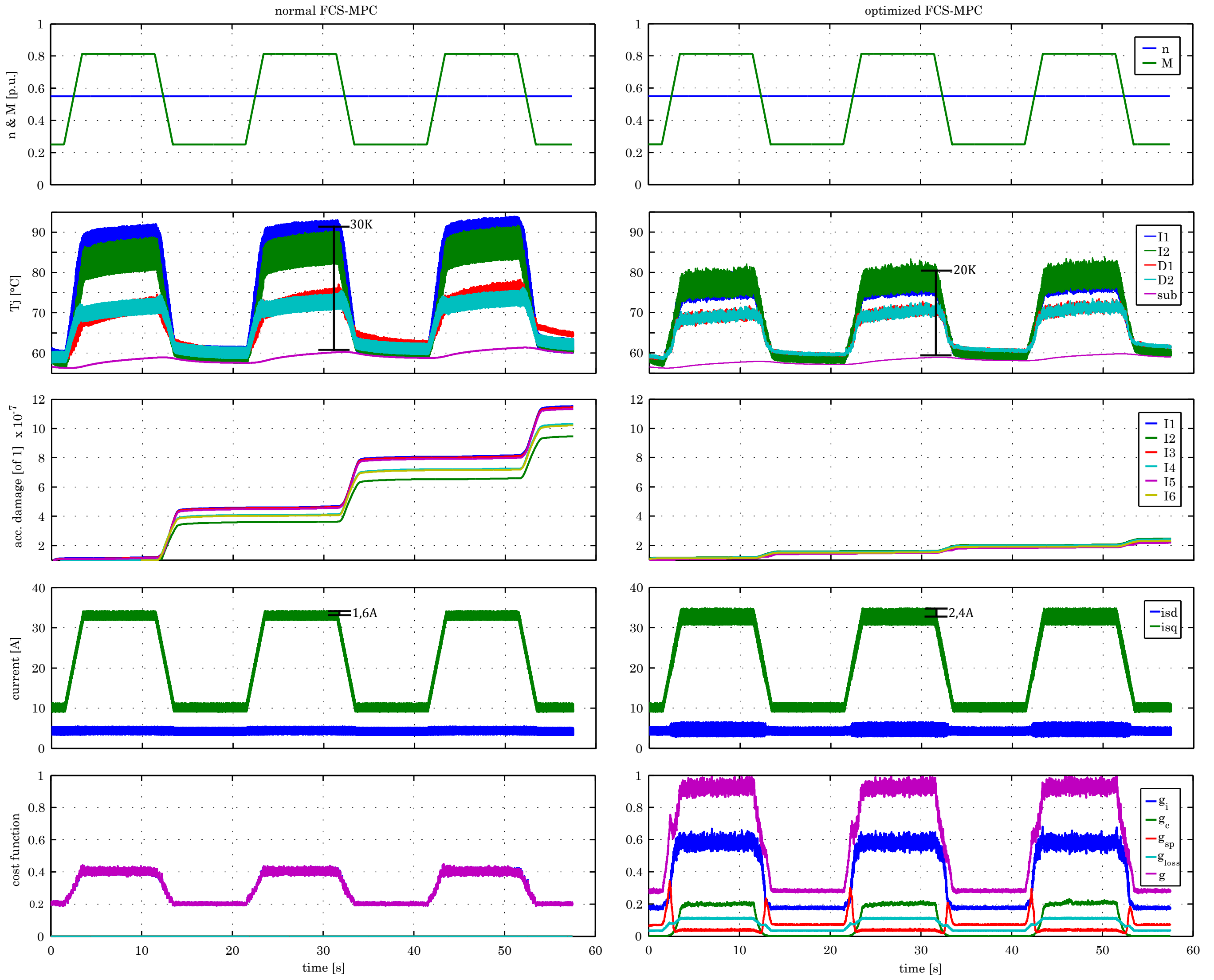

Fig. 7. Simulation of an IGBT module during a traction application mission profile. The normal FCS-MPC is given in the left column and the thermal optimized behaviour is given in the right column. Turning speed n_r and load torque M_r are given as per unit of the machine's rated operation (see table IV). First phase junction temperatures of IGBTs and diodes as well as the substrate temperature are given. The accumulated damage is calculated on basis of equation (2). In the bottom plots the values of the minimal cost function are given (lowpass filtered for viability $f_c = 100Hz$). In normal FCS-MPC only the current reference error is minimized. The cost function of the optimized FCS-MPC is weighted using the λ-parameters of table III.

TABLE IV
SIMULATION PARAMETERS

Component	**Parameter**	**Symbol**	**Value**	**Unit**
Control system	sampling time	T_s	100	μs
IGBT Module	max. voltage	V_{dc}	1.2	kV
IGBT Module	max. current	I_{max}	50	A
IGBT Module	ambient temp.	T_a	50	°C
Induction Machine	rated power	P_r	11	kW
Induction Machine	rated speed	n_r	1455	rpm
Induction Machine	rated torque	M_r	72.2	Nm

TABLE V
LIFETIME ESTIMATION FOR TRACTION MISSION PROFILE

	$T_{j,high}$	$T_{j,low}$	ΔT_j	N_f	est. lifetime
normal	93 °C	63 °C	30 K	$0.26 \cdot 10^7$	4.9 yrs
optimized	82 °C	62 °C	20 K	$1.54 \cdot 10^7$	29.4 yrs

ented control scheme using PI controllers. Inverter current and junction temperatures are controlled with the proposed thermal-based MPC. The full scheme of the 3-phase motor control is given in Fig. 2. It is used to control the motor current and optimize the thermal behavior in a three-phase IGBT module during periodic load changes of the electric drive in a traction application. The mission profile specifies motor turning speed and load torque. The turning speed is kept constant during three trapezoidal load changes per minute. The used parameters for the simulation are given in table IV.

The simulation results are given in Fig. 7. For compar-

ison, the simulation is run in normal operation and with the proposed active thermal control. In normal operation the λ-coefficients except of λ_i are set to zero and the FCS-MPC is only used to control the load current according to the references of the field oriented control. A thermal cycle amplitude of 30 K arises. In the second run of the simulation the active thermal control algorithm is included to the FCS-MPC cost function optimization. The effect of this active thermal control is a reduction of the thermal cycle amplitude to 20 K at the same boundary conditions. Using the CIPS 2008 lifetime model introduced in section III and Miner's cumulative damage rule [33] it is possible to estimate the number of runs of the mission profile to module failure. Assuming this profile is run for 8 hours per day, the lifetime can be given as numbers of years. This is done in table V. As a result, the reduction of the thermal cycle amplitude leads to an increase of the estimated lifetime by the factor of six in this simulation. The drawback is an increased amount of ripple in the stator current during the periods when the control prevents switching operations.

C. Performance and Tuning

The λ-coefficients are used to adjust the control priorities between thermal stress reduction and current ripple. To visualize the effect, a multitude of simulations have been conducted, while varying the ratio of λ_i to λ_c while the other λ-coefficients are set to zero. This varies the gain of current reference error and thermal evoked damage. The effect on on junction temperature swing, lifetime, current ripple and torque ripple are evaluated for each ratio. The temperature cycle amplitude is calculated according to Fig. 4. The remaining lifetime is calculated using the procedure of the previous paragraph and equation (2). As a measure for the current ripple, the root mean square (rms) is applied:

$$i_{s,ripple} = \sqrt{\frac{1}{n} \cdot \sum_{k=1}^{n} \left(i_s - i_{s,avg}\right)^2} \tag{12}$$

In this equation $i_{s,avg}$ is a lowpass filtered signal of the stator current i_s. The torque ripple is calculated using a measure of the electromagnetic torque:

$$T_e = \frac{2}{3} \cdot p \cdot L_m \left(i_{s,q} \cdot i'_{r,d} - i_{s,d} \cdot i'_{r,q}\right) \tag{13}$$

As a measure for the torque ripple, the RMS is applied similar to (12). The impact on junction temperature swing and current ripple is shown in Fig. 8. The derived impact on lifetime and torque ripple is shown in Fig. 9. The tradeoff of these parameters is used to find the optimal gain of the λ-coefficients that fulfills the application dependent demands. The figure shows that always a compromise between reduced stress and additional ripple must be agreed. However, adjusting of the coefficients can be seen as an additional degree of freedom in the system engineering.

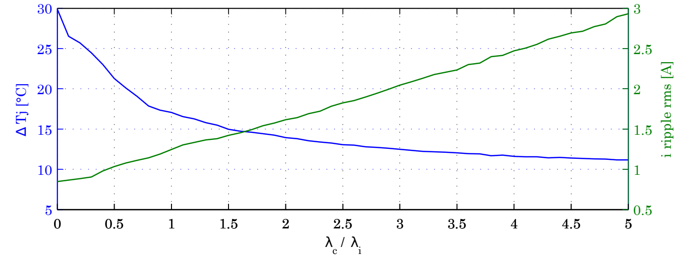

Fig. 8. Tuning of the thermal-based MPC by varying the normalized ratio λ_c to λ_i. View on temperature cycle amplitude versus RMS of ripple current.

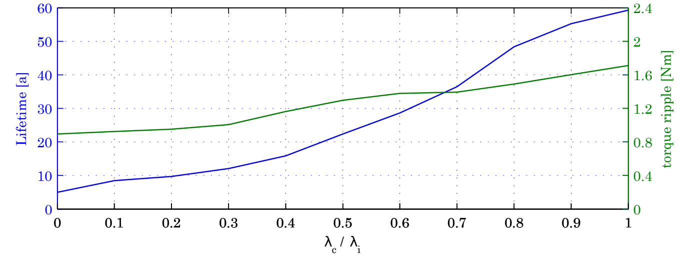

Fig. 9. Tuning of the thermal-based MPC by varying the normalized ratio λ_c to λ_i. View on lifetime (mission profile of Fig. 7) versus torque ripple.

D. Equalizing thermal stress

In this simulation, the thermal characteristics of all IGBTs are equal and no aging is assumed. However, in reality the average junction temperatures in an IGBT module may have non-tolerable differences during operation, even the converter is driven with a symmetric load. One reason is the non-symmetric design of power modules. Semiconductors that are placed next to others receive additional heat. Thus, semiconductors that are located in the middle of the module receive more heat than those that are located at the edge. Another reason is that aging of the semiconductors does not occur concurrent due to tolerances in the fabrication. Thus, the thermal characteristics and the heat transfer capability change over time.

If the first semiconductors in a module fails due to aging, is has reached end of life and the whole module has to be replaced. Consequently, if the speed of aging could be equalized, the modules lifetime would be maximized. A possibility to influence the aging of a semiconductor is to control its thermal stress.

The proposed control structure offers the possibility to relieve thermal stress from selected IGBTs or diodes. As the FCS-MPC does not use a modulator, it has direct influence on the space vector that is applied on the converter. For each space vector, the involved semiconductors are known. Consequently, the turn-on or the conducting for multiple sampling times of this semiconductor can be included to the MPC cost function as an additional penalty term. In the optimization routine of the MPC, the space vector with the lowest costs is applied to the system. Space vectors that include the selected semiconductor obtain a bias in the optimization, which results in less usage of the semiconductor. This leads to decreased power losses

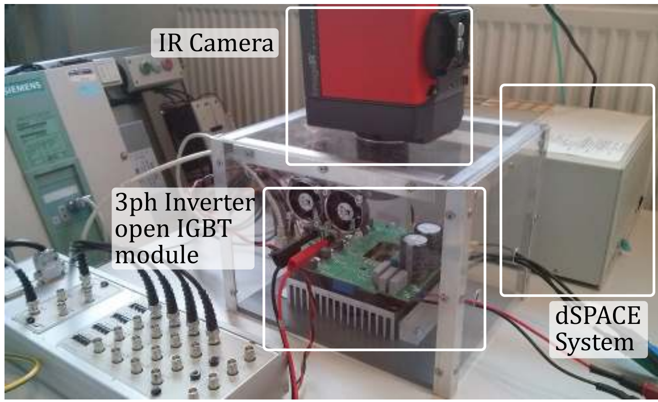

Fig. 10. Three-phase inverter experimental setup. The infrared camera is used to measure the semiconductor temperature profile of an opened IGBT module during operation.

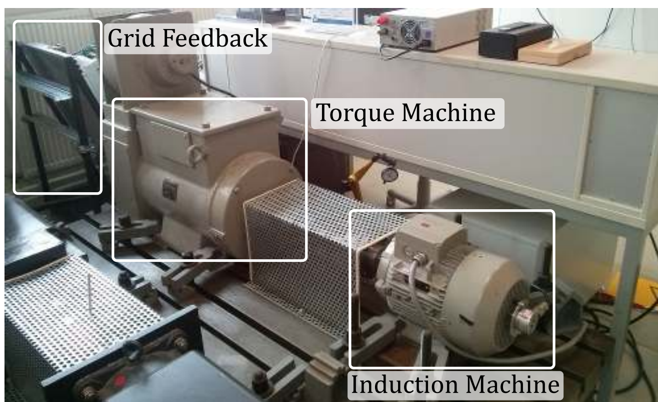

Fig. 11. Machine test bench used for experimental validation of the thermal-based FCS-MPC.

and therefore a lower average temperature. According to the Coffin-Manson-Arrhenius lifetime model, this reduces stress and thus the aging. The possibility to influence single chips on the module is demonstrated in the experimental results.

E. Experimental results

The experimental validation is done on a three-phase two-level dc/ac inverter. An open IGBT module without the use of isolating gel filling is used. This allows direct temperature measurements on the chips but decreases the isolation voltage below the rated values. For power input dc power supply is used. The load is an induction machine that is mechanical connected to a torque machine. The control is implemented on a *dSPACE DS1006* processor board. The parameters of the experimental setup are given in table VI.

For illustration of the junction temperatures in the physical setup, a high speed infrared camera is used. The thermal-based FCS-MPC algorithm has no access to the measured temperatures. It is relying on the model-based junction temperature estimation. A photograph of the measurement system is given in Fig. 10 and a photograph of the machine test bench is given in Fig. 11.

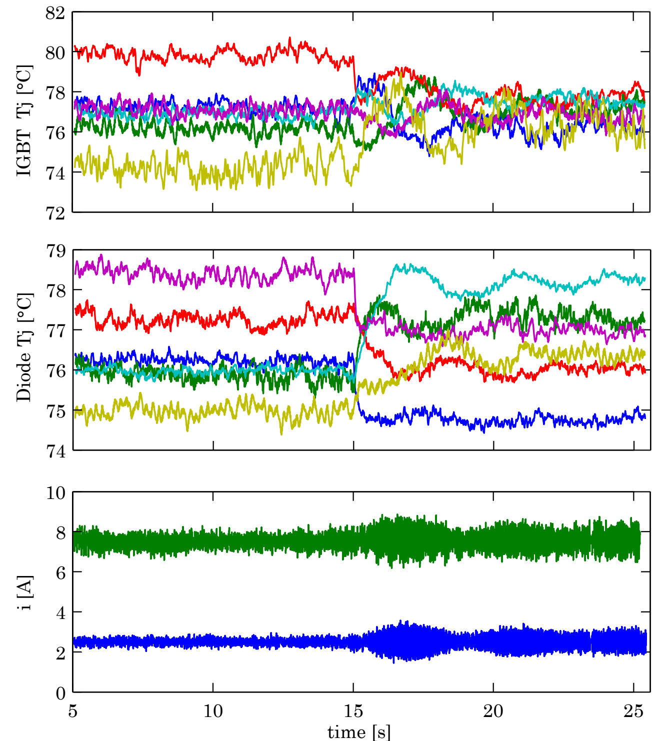

Fig. 13. Equalization of IGBT junction temperatures in a module. Measured junction temperatures of all six IGBTs and diodes in the module are shown. At t=15s the control is activated. The λ_{sp}-coefficient can be varied to decide the amount of equalization. Legend is equal to Fig. 12.

TABLE VI
EXPERIMENTAL SETUP PARAMETERS

Component	Parameter	Symbol	Value	Unit
Control system	sampling time	T_s	50	μs
IGBT Module	max. voltage	V_{dc}	1.2	kV
IGBT Module	max. current	I_{max}	25	A
Induction Machine	rated power	P_r	5.5	kW
Induction Machine	rated speed	n_r	1455	rpm
Induction Machine	rated torque	M_r	36.1	Nm
Infrared camera	used bandwidth	f_{ir}	200	Hz
Infrared camera	rated accuracy	T_{err}	$\pm$0.02	K

To validate the reduction of the thermal stress by using the proposed FCS-MPC, it has been applied on the experimental setup. In a first experiment, the stress during acceleration of the induction machine and during high torque peaks is relieved. In a second experiment it is demonstrated how the proposed FCS-MPC can be used to equalize unequal stress distributions of the semiconductors in an IGBT module. For both experiments the machine control scheme equals that one used for the simulation in Fig. 2.

1) Experiment to reduce stress: The experimental results are given in Fig. 12. As a consequence to the high gradient in the junction temperatures, the FCS-MPC is selecting switching patterns that constitute less switching losses. This can be seen in the temporary decrease of the average switching frequency during acceleration. Therefore, the amplitude of the thermal

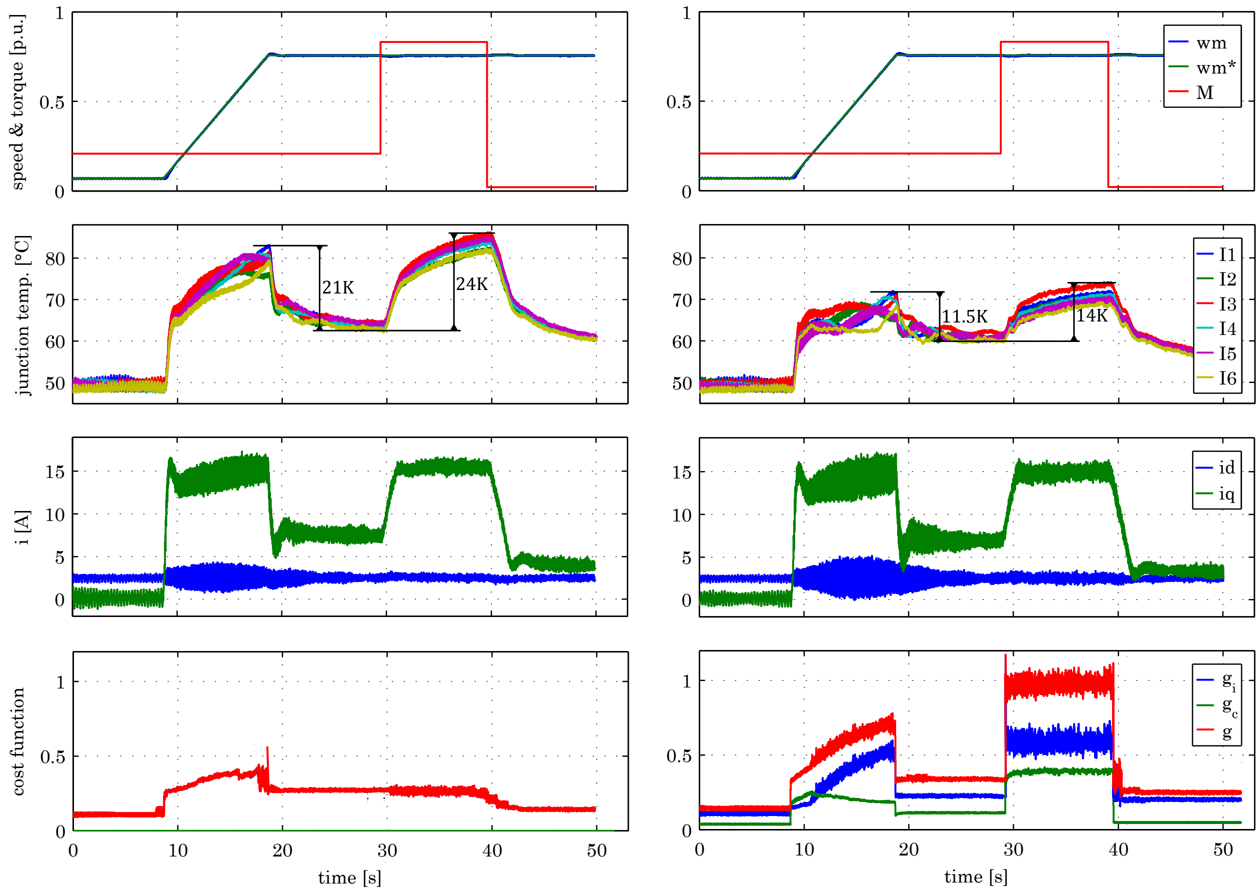

Fig. 12. Using FCS-MPC to reduce the thermal stress during acceleration and load change of an induction motor. Normal MPC is used on the left, thermal optimized MPC is used on the right. The junction temperature peaks can be reduced while the current ripple increases. In the bottom plots the values of the minimal cost function are given (lowpass filtered for viability $f_c = 100Hz$). In normal FCS-MPC only the current reference error is minimized. The cost function of the proposed FCS-MPC is optimized for minimal current reference error and thermal stress reduction.

overshoot is reduced by more than $40\,\%$.

2) Experiment to equalize stress in semiconductors: The possibility to influence single chips on the module is demonstrated. The FCS-MPC is used to equalize the temperatures of all IGBTs in the module. This has the effect that their fatigue is also more equalized.

The selection of semiconductors that receive a relief of their loading is done online using the temperature equalization element of the FCS-MPC cost function. It is used to divide the thermal stress in order to equal the average temperatures of all semiconductors.

The consequences to the other semiconductors in the module that are not relieved from stress are dependent from the control strategy that is defined by the cost function. In this case, choosing of selected space vectors is penalized. Therefore, these space vectors are avoided which results in a decrease of the average switching frequency. This is analog to well-known switching frequency reduction methods that avoid switching to other space vectors than the adjacent or zero vectors to reduce the number of commutations. If such a method is used, is has to be intermitted during the stress relieve procedure.

The results for this experiment are given in Fig. 13. The differences of the IGBT temperatures I1 to I6 are reduced. Due to the changed prioritization of space vectors also the conductivity of the power diodes D1 to D6 is affected which can be seen in the new distribution of the diode temperatures. The drawback of this technique is an increase in the current ripple. As some space vectors are used less frequently, this additional ripple occurs.

V. Conclusion

The MPC offers the possibility to include non-linear statements to the control. The FCS-MPC additional offers the possibility to specify the exact switching sequence of the IGBT converter. Both of these properties are well-suited to improve the effectiveness of active thermal control, which is used to reduce the thermal stress in the semiconductor devices. It allows calculating the additional fatigue that an arising thermal cycle adds on each individual chip during inverter operation using a prediction model. This information is considered in the the MPC cost function optimization in order to minimize the thermal stress individually for each chip. Consequently, the FCS-MPC enables to re-distribute the thermal stress in the chips. In the experiment the thermal cycling could be reduced by more than $40\,\%$ and the spread between lowest

and highest IGBT junction temperature could be reduced from $7\,\mathrm{K}$ to $3\,\mathrm{K}$. This is used to equalize the aging of the chips. Considering that the first failed device in a module ends its lifetime, this technique enables to improve the module lifetime. The variation of the cost function element coefficients is an additional degree of freedom in the system design. It allows a trade-off between reducing the thermal stress and additional ripple in current or torque.

Acknowledgment

The research leading to these results has received funding from the Gesellschaft für Energie und Klimaschutz Schleswig-Holstein GmbH (EKSH) doctoral studies grant.

References

[1] S. Kouro, M. Perez, J. Rodriguez, A. Llor, and H. Young, "Model predictive control: Mpc's role in the evolution of power electronics," *IEEE Industrial Electronics Magazine*, vol. 9, no. 4, pp. 8–21, Dec 2015.

[2] H. Wang, M. Liserre, and F. Blaabjerg, "Toward reliable power electronics: Challenges, design tools, and opportunities," *IEEE Industrial Electronics Magazine*, vol. 7, no. 2, pp. 17–26, June 2013.

[3] B. Ji, X. Song, E. Sciberras, W. Cao, Y. Hu, and V. Pickert, "Multiobjective design optimization of igbt power modules considering power cycling and thermal cycling," *IEEE Transactions on Power Electronics*, vol. 30, no. 5, pp. 2493–2504, May 2015.

[4] A. Wintrich, U. Nicolai, W. Tursky, and T. Reimann, "Semikron, application manual power semiconductors," *Ilmenau: ISLE*, 2011.

[5] A. Volke and M. Hornkamp, *IGBT modules: technologies, driver and application*, 2nd ed. Infineon Technologies AG, 2012.

[6] M. Schulz, "Thermal management details and their influence on the aging of power semiconductors," in *Proc. of 2014 16th European Conference on Power Electronics and Applications (EPE'14-ECCE Europe)*. IEEE, 2014, pp. 1–6.

[7] M. Andresen, K. Ma, G. Buticchi, J. Falck, F. Blaabjerg, and M. Liserre, "Junction temperature control for more reliable power electronics," *IEEE Transactions on Power Electronics*, vol. 33, no. 1, pp. 765–776, Jan 2018.

[8] D. Murdock, J. Torres, J. Connors, and R. Lorenz, "Active thermal control of power electronic modules," *IEEE Transactions on Industry Applications*, vol. 42, no. 2, pp. 552–558, March 2006.

[9] M. Weckert and J. Roth-Stielow, "Chances and limits of a thermal control for a three-phase voltage source inverter in traction applications using permanent magnet synchronous or induction machines," in *Proc. of 2011 14th European Conference on Power Electronics and Applications (EPE 2011)*, Aug 2011, pp. 1–10.

[10] J. Lemmens, J. Driesen, and P. Vanassche, "Dynamic dc-link voltage adaptation for thermal management of traction drives," in *Proc. of 2013 IEEE Energy Conversion Congress and Exposition (ECCE)*, Sept 2013, pp. 180–187.

[11] K. Ma, M. Liserre, and F. Blaabjerg, "Reactive power influence on the thermal cycling of multi-mw wind power inverter," *IEEE Transactions on Industry Applications*, vol. 49, no. 2, pp. 922–930, March 2013.

[12] J. Zhang, Y. Li, H. Wang, X. Cai, S. Igarashi, and Z. Wang, "Thermal smooth control based on orthogonal circulating current for multi-mw parallel wind power converter," in *2014 International Power Electronics and Application Conference and Exposition*, Nov 2014, pp. 146–151.

[13] M. Bakhshizadeh, K. Ma, P. C. Loh, and F. Blaabjerg, "Indirect thermal control for improved reliability of modular multilevel converter by utilizing circulating current," in *Proc. of 2015 IEEE Applied Power Electronics Conference and Exposition (APEC)*, March 2015, pp. 2167–2173.

[14] P. K. Prasobhu, G. Buticchi, S. Brueske, and M. Liserre, "Gate driver for the active thermal control of a dc/dc gan-based converter," in *Proc. of 2016 IEEE Energy Conversion Congress and Exposition (ECCE)*, 2016.

[15] F. Hahn, G. Buticchi, and M. Liserre, "Active thermal balancing for modular multilevel converters in hvdc applications," in *Proc. of 17th International Scientific Conference on Electric Power Engineering (EPE)*, 2016.

[16] M. Andresen, G. Buticchi, J. Falck, M. Liserre, and O. Muehlfeld, "Active thermal management for a single-phase h-bridge inverter employing switching frequency control," in *Proc. of PCIM Europe 2015; International Exhibition and Conference for Power Electronics, Intelligent Motion, Renewable Energy and Energy Management*, May 2015, pp. 1–8.

[17] J. Holtz and S. Stadtfeld, "A predictive controller for the stator current vector of ac machines fed from a switched voltage source," in *Proc. of JIEE IPEC-Tokyo Conference*, 1983, pp. 1665–1675.

[18] J. Rodriguez, M. Kazmierkowski, J. Espinoza, P. Zanchetta, H. Abu-Rub, H. Young, and C. Rojas, "State of the art of finite control set model predictive control in power electronics," *IEEE Transactions on Industrial Informatics*, vol. 9, no. 2, pp. 1003–1016, May 2013.

[19] E. F. Camacho and C. B. Alba, *Model predictive control*. Springer Science & Business Media, 2013.

[20] L. Wang, *Model predictive control system design and implementation using MATLAB*. Springer Science & Business Media, 2009.

[21] M. Andresen and M. Liserre, "Impact of active thermal management on power electronics design," *Microelectronics Reliability*, vol. 54, no. 9, pp. 1935–1939, 2014.

[22] T. Herrmann, M. Feller, J. Lutz, R. Bayerer, and T. Licht, "Power cycling induced failure mechanisms in solder layers," in *Proc. of 2007 European Conference on Power Electronics and Applications*, Sept 2007, pp. 1–7.

[23] N. Baker, M. Liserre, L. Dupont, and Y. Avenas, "Junction temperature measurements via thermo-sensitive electrical parameters and their application to condition monitoring and active thermal control of power converters," in *Proc. of 39th Annual Conference of the IEEE Industrial Electronics Society, IECON 2013*, Nov 2013, pp. 942–948.

[24] J. Falck, M. Andresen, and M. Liserre, "Active thermal control of igbt power electronic converters," in *Proc. of 2015 41st Annual Conference of the IEEE Industrial Electronics Society (IECON)*. IEEE, 2015, pp. 1–6.

[25] A. Wintrich, U. Nicolai, W. Tursky, and T. Reimann, *Application Manual Power Semiconductors*, 2nd ed., ISLE, Ed. Semikron, 2015.

[26] H. Cui, "Accelerated temperature cycle test and coffin-manson model for electronic packaging," in *Annual Reliability and Maintainability Symposium, 2005. Proceedings.*, Jan 2005, pp. 556–560.

[27] F. Blaabjerg, K. Ma, and D. Zhou, "Power electronics and reliability in renewable energy systems," in *Proc. of IEEE International Symposium on Industrial Electronics (ISIE)*. IEEE, 2012, pp. 19–30.

[28] R. Bayerer, T. Herrmann, T. Licht, J. Lutz, and M. Feller, "Model for power cycling lifetime of igbt modules - various factors influencing lifetime," in *Proc. of 5th International Conference on Integrated Power Systems (CIPS)*. VDE, 2008, pp. 1–6.

[29] H. Huang and P. A. Mawby, "A lifetime estimation technique for voltage source inverters," *IEEE Transactions on Power Electronics*, vol. 28, no. 8, pp. 4113–4119, Aug 2013.

[30] S. Kouro, P. Cortes, R. Vargas, U. Ammann, and J. Rodriguez, "Model predictive control: A simple and powerful method to control power converters," *IEEE Transactions on Industrial Electronics*, vol. 56, no. 6, pp. 1826–1838, June 2009.

[31] M. Musallam and C. M. Johnson, "An efficient implementation of the rainflow counting algorithm for life consumption estimation," *IEEE Transactions on Reliability*, vol. 61, no. 4, pp. 978–986, 2012.

[32] M. Preindl, E. Schaltz, and P. Thogersen, "Switching frequency reduction using model predictive direct current control for high-power voltage source inverters," *IEEE Transactions on Industrial Electronics*, vol. 58, no. 7, pp. 2826–2835, July 2011.

[33] I. Kovacevic, U. Drofenik, and J. Kolar, "New physical model for lifetime estimation of power modules," in *Proc. of 2010 International Power Electronics Conference (IPEC)*, June 2010, pp. 2106–2114.